Open Archive TOULOUSE Archive Ouverte (OATAO)

OATAO is an open access repository that collects the work of Toulouse researchers and makes it freely available over the web where possible.

Any correspondance concerning this service should be sent to the repository administrator: staff-oatao@listes-diff.inp-toulouse.fr

Surfactant-free CZTS nanoparticles as building blocks for low-cost solar cell absorbers

O Zaberca[1]**, F Oftinger**[1]**, J Y Chane-Ching**[1]**, L Datas**[1]**, A Lafond**[2]**,
P Puech**[3]**, A Balocchi**[4]**, D Lagarde**[4] **and X Marie**[4]

[1] Université de Toulouse, CNRS-UPS-INPT, CIRIMAT, 118 route de Narbonne, F-31062 Toulouse, France
[2] Institut des Matériaux Jean Rouxel, Université de Nantes, CNRS, 2 rue de la Houssinière, F-43322 Nantes Cedex 3, France
[3] Université de Toulouse, CNRS, CEMES, 29 rue Jeanne Marvig, F-31055 Toulouse Cedex 4, France
[4] Université de Toulouse, INSA-CNRS-UPS, LPCNO, 135 avenue Rangueil, F-31077 Toulouse, France

E-mail: chane@chimie.ups-tlse.fr

Abstract
A process route for the fabrication of solvent-redispersible, surfactant-free Cu_2ZnSnS_4 (CZTS) nanoparticles has been designed with the objective to have the benefit of a simple sulfide source which advantageously acts as (i) a complexing agent inhibiting crystallite growth, (ii) a surface additive providing redispersion in low ionic strength polar solvents and (iii) a transient ligand easily replaced by an carbon-free surface additive. This multifunctional use of the sulfide source has been achieved through a fine tuning of $((Cu^{2+})_a(Zn^{2+})_b(Sn^{4+})_c(Tu)_d(OH^-)_e)^{t+}$, Tu = thiourea) oligomers, leading after temperature polycondensation and S^{2-} exchange to highly concentrated ($c > 100 \, \text{g} \, l^{-1}$), stable, ethanolic CZTS dispersions. The good electronic properties and low-defect concentration of the sintered, crack-free CZTSe films resulting from these building blocks was shown by photoluminescence investigation, making these building blocks interesting for low-cost, high-performance CZTSe solar cells.

1. Introduction

Copper–zinc–tin chalcogenide (Cu_2ZnSnS_4, CZTS) materials have attracted increasing attention for solar cell absorber layers [1, 2]. In contrast to well-known solar absorber materials for thin film chalcogenide-based solar cells such as $Cu(In, Ga)(S, Se)_2$ and CdTe, CZTS is composed of abundant [3] and non-toxic elements. The direct bandgap of this material (1.45–1.6 eV) [4, 5] falls within the optimum range for a single-junction terrestrial solar cell. In addition, this material possesses a large band edge absorption coefficient of about $10^4 \, \text{cm}^{-1}$ [4]. Initial attempts to fabricate photovoltaic devices using CZTS material involved evaporation of elemental Cu/Sn/Zn structures

and subsequent sulfurization at $500 \,^{\circ}\text{C}$ using nitrogen with 5% H_2S atmosphere [2]. Then, various deposition methods for CZT(S, Se) films were proposed including sputtering processes [4–6], electro-deposition [7, 8] or the ink printing route [9, 10]. This latter process has been developed to address the issue of fabrication costs, replacing potentially more expensive vacuum-based techniques. In the context of the CZTSe film fabrication by nanoparticle printing, the most successful work has been developed by the IBM group involving the use of Cu_2S, ZnSe and SnSe binary chalcogenide building blocks dispersed in hydrazine solvent [11]. Use of quaternary chalcogenide CZTS nanoparticles which potentially presents the advantage of a higher chemical homogeneity of the resulting sintered CZTSe

film was also proposed [9–12]. In those works, the reported CZTS nanocrystal synthetic route generally involves the use of a coordinating solvent such as oleylamine [9–13] or surfactants [14]. All these synthetic routes invariably result in CZTS nanoparticles displaying nearly spherical morphology with particle sizes ranging from 15 to 30 nm. Although these process routes have already demonstrated their potential to produce CZTS nanoparticles exhibiting appropriate properties for the fabrication of high-performance solar cells with yields up to 9.66% [12], the industrial development of the nanoparticle printing route will probably rely on the successful fabrication of an absorber layer via a high-throughput process [15]. In this context, the determination of the CZTS nanocrystals' optimal characteristics for the high-throughput ink printing route will require the design of new nanoparticle synthetic routes. Indeed, the ability to control crystallinity, morphology and size of the CZTS nanocrystals will provide us with an opportunity to further test the effects of these characteristics on forming and sintering behaviors. Among process routes leading to the formation of nanoparticles usually developed in the case of oxide nanoparticles, various strategies have already been reported such as the use of preformed nanoreactors achieved from surfactants [16] or ligands [17], controlled de-complexation reactions [18] or polycondensation reactions involving specifically designed ionic or oligomeric precursors [19]. In these latter process routes, nanocrystal formation generally occurs by temperature and autogenous pressure-activated hydrothermal or solvothermal reactions [19]. In the context of chalcogenide nanoparticle fabrication, previous works involving precipitation of $CuInS_2$ ternary chalcogenide from a sulfide source interacting directly with Cu^{x+} and In^{3+} cations have demonstrated that solvothermal routes usually result in micron-sized particles [20–22].

Here, we demonstrate the production of solvent-dispersible CZTS nanocrystals via a high temperature poly-condensation route involving $((Cu^{2+})_a (Zn^{2+})_b(Sn^{4+})_c (Tu)_d (OH^-)_e)^{t+}$ ($Tu = CS(NH_2)_2$, thiourea) tailored complex precursors. We show that our process route indeed combines both arrested polycondensation of $((Cu^{2+})_a (Zn^{2+})_b(Sn^{4+})_c (Tu)_d (OH^-)_e)^{t+}$ oligomers and transformation of SnO_2-based preformed nanoreactors. The simple synthetic route we have developed to produce surfactant-free CZTS nanocrystals yields partially crystallized nanoparticles. Design of complex precursors as well as protocol optimization were carried out with the objective to fully take the benefit of the sulfide source thiourea as a complexing agent for growth inhibition and as a surface additive for redispersion in polar solvents. Crack-free CZTS green films were achieved using these nanoparticles by dip coating of an ethanolic dispersion yielding, after sintering under Se atmosphere, CZTSe films possessing a low-defect concentration as shown by photoluminescence spectroscopy. Thus, these partially crystallized CZTS nanoparticles represent attractive building blocks for the realization of crack-free sintered films for high-performance CZTS solar cells.

2. Experimental details

2.1. Synthesis of CZTS nanocrystals

Polycondensation reactions at 200 °C were performed in ethylene glycol, ethanol and isopropanol using $CuCl_2$ xH_2O, $SnCl_4$, $5H_2O$ and $ZnCl_2$ as metallic salts and respectively thiourea and tetra methyl ammonium hydroxide (TMaOH) as sulfide and OH^- sources [23]. Because of the low solubility of CuCl, $CuCl_2$ was employed to improve chemical homogeneity of the precursors. Production of small crystallite size was promoted by achieving high supersaturation conditions through ascorbic acid addition, yielding an increase of $[Cu^+]$ when employing non-reductive solvents such as ethanol or isopropanol. Various compositions of reaction mixtures close to the stoichiometric composition were investigated. Composition of the reaction mixtures was defined in molar ratios $(Cu:Zn:Sn:S:OH) = (x_{Cu}:x_{Zn}: x_{Sn}:x_S:x_{OH})$, where x_{Cu}, x_{Zn}, x_{Sn}, x_S and x_{OH} represent respectively the total number of copper, zinc, tin, sulfur and OH moles incorporated into the reaction mixture. A rational investigation of starting compositions was performed by variation of both the OH partial neutralization rate and the sulfide over stoichiometry. Two crucial parameters could thus be defined, $n_{OH} = (OH)_{prec}/(OH)_{stoic}$ and $n_s = [S]/[Cu]$. In these equations, $(OH)_{prec}$ and $(OH)_{stoic}$ denote respectively the OH moles involved in the precursor preparation and the stoichiometric OH moles corresponding to the precipitation of the various cations into metallic oxy-hydroxides. [S] refers to the total sulfur concentration, $[S] = [CS(NH_2)_2]+[HS^-]+ [S^{2-}]$ and [Cu] to the total Cu concentration, $[Cu] = ([Cu^+]+ [Cu^{2+}])$ in the reaction mixtures. In the following, we have normalized the compositions by [OH]/[Cu] and [S]/[Cu] ratios.

In a typical experiment, $(Cu:Zn:Sn:S:OH) = (2.0:1.3: 1.1:10:2.0)$, Cu_2ZnSnS_4 particles are synthesized in ethylene glycol as follows: 1.73 g $SnCl_4.5H_2O$ (4.95 mmol), 0.8 g $ZnCl_2$ (5.85 mmol) and 1.534 g $CuCl_2.2H_2O$ (9 mmol) are added to 200 ml of ethylene glycol under stirring at room temperature. After complete dissolution of the metallic salts, 3.42 g $CS(NH_2)_2$ Fluka Aldrich (45 mmol) are incorporated into the solution. After stirring for 10 min at room temperature, 3.645 ml TMaOH 25% (9 mmol) is poured into the mixture then stirred for about 30 min and finally diluted to 300 ml by ethylene glycol. The resulting solution is loaded into a 1000 ml Teflon-lined steel autoclave and transferred into an oven preheated to the desired temperature. The autoclave is maintained at 200 °C for 16 h and then cooled to room temperature naturally. Samples are subsequently washed three times with 300 ml deionized water, then finally with 300 ml ethanol. The as-prepared material is finally collected by centrifugation and dried at room temperature.

2.2. Film forming and sintering

Films were formed from concentrated dispersions using CZTS nanoparticles synthesized in ethylene glycol with [OH]/[Cu] = 1 and [S]/[Cu] = 5. S^{2-} ligand exchange was carried out under air using $(NH_4)_2S$ aqueous solution. For a

typical ligand exchange, the molar ratio was $S^{2-}/CZTS = 2$. Films were formed on Mo-coated glass substrates using $100\ \mathrm{g}\ \mathrm{l}^{-1}\ S^{2-}$-capped CZTS nanoparticle dispersions. Nine layers were dip-coated at $v = 26\ \mathrm{cm}\ \mathrm{min}^{-1}$. Intermediate heat treatments carried out at $400\,^{\circ}\mathrm{C}$ under Ar were performed after three successive coatings. Films were finally sintered under Se atmosphere [6] in a quartz box at $T = 550\,^{\circ}\mathrm{C}$ for 1 h.

2.3. Material characterization

2.3.1. X-ray diffraction. Crystallographic information on CZTS crystals was obtained on a Brucker AXS D4 diffractometer operating in the Bragg configuration, using a monochromatized Cu Kα radiation ($\lambda = 1.540\,596$ Å). Diffraction patterns were collected from $2\theta = 10°$ to $70°$ at a scanning rate of $4°\ \mathrm{min}^{-1}$ with a step size of $0.025\,^{\circ}\mathrm{C}$. Diffraction patterns were compared to a reference pattern recorded from a highly crystallized, stoichiometric CZTS reference sample we have prepared at $750\,^{\circ}\mathrm{C}$ in a evacuated silica tube. Ordered domains or crystallite sizes were determined from the Scherrer equation using the full width at half-maximum of the chalcogenide (112) peak.

2.3.2. Electrophoretic mobility and particle size distribution. Electrophoretic mobility and size of the nanocrystal dispersions were measured using a Malvern Nano ZS 90 on $1\ \mathrm{g}\ \mathrm{l}^{-1}$ CZTS dispersed in ethanol.

2.3.3. Infrared spectroscopy. The infrared spectra of CZTS crystals were recorded using a Perkin Elmer 1760-X FTIR spectrometer. The spectra were recorded on potassium bromide discs in the range 4000–400 cm^{-1}.

2.3.4. Raman spectroscopy. Micro-Raman measurements were performed using a Horiba Jobin Yvon XPlora equipped with an Olympus microscope. A 50× objective and low laser power ($0.01\ P_{\mathrm{o}}$) have been used to avoid any thermal effects due to laser heating. With $0.1\ P_{\mathrm{o}}$ laser power, downshift of the Raman bands due to heating was observed while the spectra remain identical with 0.1%. The laser output powers at 515 nm, 638 nm and 785 nm were $P_{\mathrm{o}} = 15$ mW, 15 mW and 40 mW, respectively. The focused spot diameter on the samples was ~1 μm leading with the reported spectra at 785 nm to an excitation power of 0.5 mW μm^{-2}.

2.3.5. Elemental analysis. Chemical analysis was conducted by ICP-AES (Service Central d'Analyses du CNRS, Solaize, France) or by energy dispersive x-ray spectroscopy (EDS) (Hitachi S-4000 field emission scanning electron microscope) on powder cast as pellets. The microscope operated at an electron acceleration voltage of 20 kV. The precision of the EDS elemental analysis was determined from a reference sample displaying stoichiometric composition as shown by chemical analysis. Quantitative estimates of elements were made by averaging five values.
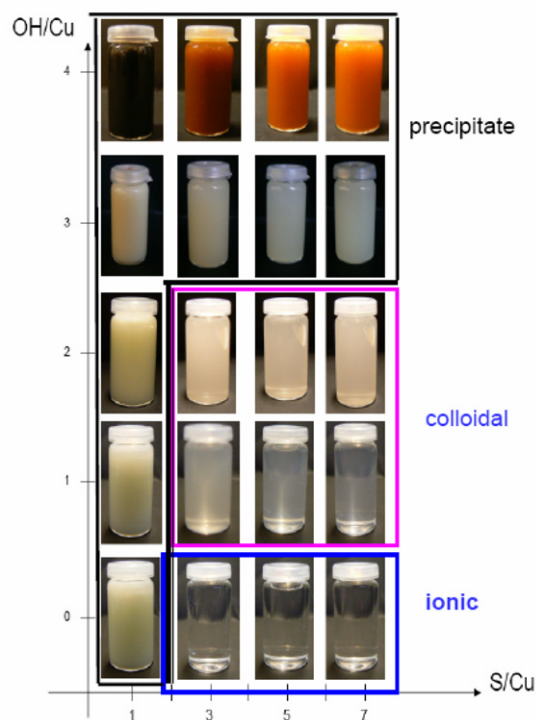
Figure 1. Ionic, colloidal and precipitation domains of CZTS precursors in ethylene glycol.

2.3.6. Electron microscopy. Specimens for low magnification transmission electron microscopy (TEM) and high resolution transmission electron microscopy (HRTEM) were obtained by drying droplets of a CZTS sample from an ethanolic dispersion onto a 300-mesh Cu grid, coated with a lacey carbon film. TEM images were taken at an accelerating voltage of 100 kV on a JEM 1011. HRTEM images were obtained on a JEOL JEM 2100 F at an accelerating voltage of 200 kV.

2.4. Photoluminescence

Time-resolved photoluminescence experiments were performed using a mode-locked Ti:Sa laser with 1.2 ps pulse duration and 80 MHz repetition frequency, at a wavelength $\lambda = 760$ nm and average power $P_{\mathrm{ave}} = 50$ mW, focused to a 50 μm diameter spot. The PL dynamics were recorded with a S1 photocathode Hamamatsu synchroscan streak camera C 5680 with 15 ps overall time resolution.

3. Results and discussion

3.1. Fine-tuning of CZTS precursor characteristics

Figure 1 displays the large family of precursors prepared in ethylene glycol including ionic solutions ($n_{\mathrm{OH}} < 0.1$), colloidal dispersions ($0.1 < n_{\mathrm{OH}} < 0.50$) and agglomerate suspensions ($0.5 < n_{\mathrm{OH}}$) depending on OH addition in a very limited range. These agglomerates were shown to be mainly Sn^{4+}-based compounds as shown from the XRD investigation performed on the corresponding calcined precipitates. Indeed, after heat treatment under N$_2$ atmosphere at $T = 550\,^{\circ}\mathrm{C}$, these precipitates were identified as SnS$_2$ and SnS compounds.
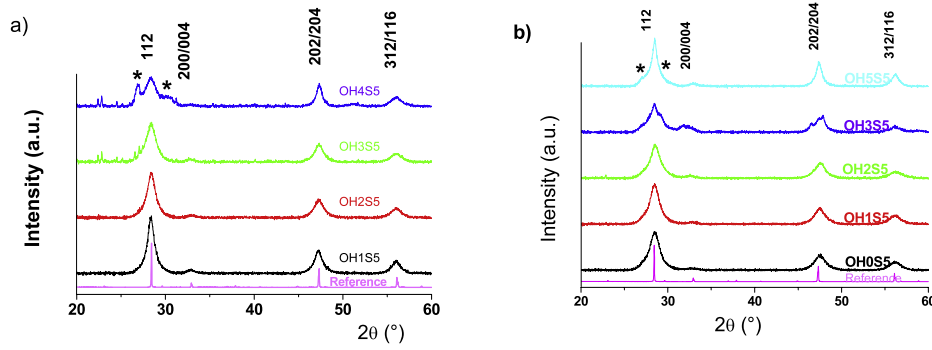
Figure 2. XRD patterns of samples displaying peaks corresponding to the Cu_2ZnSnS_4 tetragonal phase. (a) Samples prepared in isopropanol at $200\,°C$ for various $x = [OH]/[Cu]$ and $y = [S]/[Cu]$ compositions. $(Cu:Zn:Sn:S:OH) = (2.0:1.25:1.0:x:y)$. (b) Samples prepared in ethylene glycol at $200\,°C$ for $x = [S]/[Cu] = 5$. $(Cu:Zn:Sn:S:OH) = (2.0:1.3:1.1:x:y)$. Samples prepared at $[OH]/[Cu] = x$ and $[S]/[Cu] = y$ are denoted OH_xS_y. CZTS assignments are made from the well-crystallized powder (reference). * Indicates peak assigned to the ZnS wurtzite structure.

Formation domains of ionic, colloidal and precipitates precursors were also determined in ethanol and isopropanol solvents. Similarly, the same evolution from ionic → colloidal → precipitates precursors was observed for increased [OH]/[Cu] values.

3.2. Partially crystallized CZTS particles

The formation conditions of samples exhibiting x-ray diffraction peaks which can be assigned to the Cu_2ZnSnS_4 tetragonal phase were investigated in ethylene glycol and isopropanol at $T = 200\,°C$ under autogenous pressures [23]. In comparison with conventional approaches involving reactions between metallic cations and a sulfide source [21, 22], fine inspection of the formation diagrams indicates a significant extension of the single tetragonal phase formation domains with OH^- addition. XRD patterns of samples synthesized for stoichiometric $(Cu:Zn:Sn) = (2.0:1.0:1.0)$, or copper-deficient reaction mixture compositions $(Cu:Zn:Sn) = (2.0:1.25:1.0)$ in isopropanol and in ethylene glycol $(Cu:Zn:Sn) = (2.0:1.3:1.1)$ show a small formation domain of the tetragonal phase $(n_{OH} < 0.4, 2 < n_s < 7)$ (figure 2). Reaction mixtures with higher values of [OH]/[Cu] in ethylene glycol result in the formation of wurtzite ZnS in association with the CZTS tetragonal structure. Indeed, formation of crystals exhibiting a single CZTS phase was achieved from polycondensation of ionic solutions or colloidal dispersion complex precursors. In the whole range of reaction mixture compositions investigated, similar cell parameters $(a = b = 5.431\,Å, c = 10.826\,Å)$ corresponding to the CZTS cell parameters were determined. Ordered domain sizes ranging from 5 to 20 nm were determined as calculated from the Scherrer equation using the full width at half-maximum of the chalcogenide (112) peak. Because these ordered domains could be identified with individual nanocrystals as shown later on by HRTEM, these low values indicate a high supersaturation regime for the CZTS formation, suggesting high $[Cu^+]$ and $[S^2]$ concentrations, due respectively to the efficient reductive effect of ethylene glycol or ascorbic acid and the easy formation of sulfide anions from $CS(NH_2)_2$ with OH^- additions.

As previously reported [24, 25], complete identification of the CZTS structure cannot be obtained from an x-ray investigation since β-ZnS and Cu_3SnS_4 structures cannot be distinguished easily from the Cu_2ZnSnS_4 structure. Raman spectroscopy was shown to be a powerful technique to clarify the presence of these secondary phases. Our preliminary investigations have shown that the laser excitation wavelength significantly affects the Raman spectra features recorded on CZTS samples synthesized in ethylene glycol and isopropanol at $T = 200\,°C$. Using red excitation $(\lambda = 638\,nm)$, huge luminescence intensity is recorded while with green excitation $(\lambda = 515\,nm)$, we observe at first some residual luminescence signal and secondly a strong signal at $336\,cm^{-1}$ which is assigned to CZTS (see below). Quasi-complete removal of the luminescence contribution was achieved using a near infrared wavelength laser excitation $(\lambda = 785\,nm)$. Because this excitation energy is just below the bandgap, amorphous and crystallized domains of the sample are probed together within the spot size with a depth defined by the objective and the real index of the composite material.

The Raman spectra recorded with an infrared laser excitation on various CZTS samples prepared in isopropanol and ethylene glycol at $T = 200\,°C$ for samples exhibiting a single tetragonal phase by XRD are reported figure 3. Large differences were observed depending mainly on n_{OH} and n_s ratios with large variations in the background intensity.

The spectrum recorded on the sample prepared at $[S]/[Cu] = 7$ exhibits features corresponding mainly to amorphous material. Indeed, the observed decrease of the background with frequency is usually associated with amorphous materials. In addition, the corresponding Raman signal is composed of a contribution proportional to the one-phonon density of states and a poorly structured contribution due to multi-order Raman scattering [26, 27]. For these samples prepared at high [S]/[Cu] values, the larger intensity of the background signal indicates a larger amorphous phase proportion. In contrast, Raman spectra of samples prepared at $[S]/[Cu] = 5$ give more defined signals, revealing the presence of small nanocrystals embedded in an amorphous phase. For these samples, the full width at half-maximum (FWHM) of the main contribution is a good
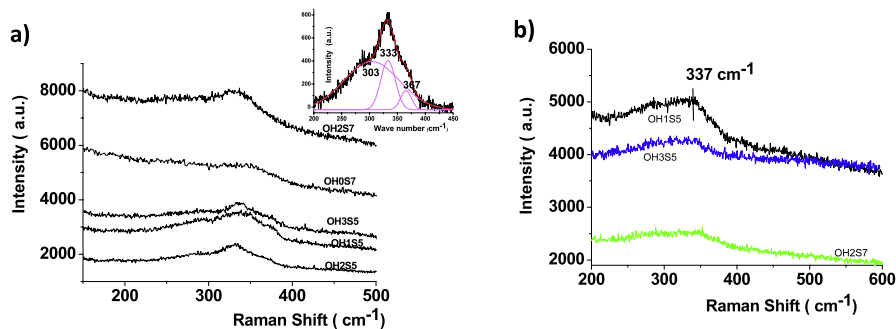
Figure 3. (a) Raman spectra of CZTS samples synthesized in ethylene glycol at 200 °C. Large differences are observed in the background signal intensity of the various spectra indicating various amorphous phase proportions in the samples. Inset: deconvolution of the Raman broad peak in the 250–400 cm^{-1} domain recorded on sample synthesized at [OH]/[Cu] = 2 and [S]/[Cu] = 5 highlighting a main peak and secondary peaks assigned to bulk CZTS. (b) Raman spectra of CZTS crystals synthesized in isopropanol at 200 °C.

Table 1. Raman characteristics of CZTS particles prepared in ethylene glycol at 200 °C: reported peak maximum wavenumber and FWHM were determined after deconvolution of the broad Raman peak in the 250–400 cm^{-1} domain.

	Peak 1		Peak 2		Peak 3	
	Max. (cm^{-1})	FWHM (cm^{-1})	Max. (cm^{-1})	FWHM (cm^{-1})	Max. (cm^{-1})	FWHM (cm^{-1})
OH1S5	341	46	291	102	372	13
OH2S5	333	26	303	98	365	20
OH3S5	338	31	296	140	367	24
OH0S7	321	95	259	32	352	55
OH2S7	338	50	285	105		

indicator of the size and/or the crystallinity of the embedded nanocrystals. Thus, simulation and deconvolution of the broad peak in the 250–400 cm^{-1} domain were performed using multiple Lorentzian functions involving three peaks fixed around 286 , 336 and 362 cm^{-1} assigned to bulk CZTS [28]. Raman shift values, similar to data previously reported for bulk CZTS, were determined for these samples prepared at [S]/[Cu] = 5. Using the FWHM value of the main peak as a criterion, reaction mixtures close to [S]/[Cu] = 5 and [OH]/[Cu] = 2 were selected as optimal conditions for the CZTS crystal preparation (table 1).

Although isopropanol solvent yields larger autogenous pressure compared to ethylene glycol during polyconden-sation reactions operating at T = 200 °C, Raman spectra of the CZTS crystals prepared in isopropanol exhibit less well-resolved peaks, highlighting a better formation of the CZTS structure in ethylene glycol.

### 3.3. CZTS particle composition: thiourea–metal complexes

A large Zn deficiency was determined from chemical analysis of CZTS samples synthesized in ethanol (table 2). Surprisingly, for similar reaction mixture compositions, Zn incorporation was better achieved when using isopropanol as solvent. Nevertheless, nearly stoichiometric compositions displaying smaller Zn and Sn deficiencies were better achieved in ethylene glycol. In addition, CZTS nanocrystals displaying nonstoichiometric Cu/(Zn + Sn) and Zn/Sn molar

Table 2. Chemical composition of CZTS samples prepared from polycondensation of complex precursors in various solvents (ethanol, isopropanol and ethylene glycol) at 200 °C–16 h. (1) Data from chemical analysis. (2) Data from energy dispersive x-ray spectroscopy (EDS) analysis. Only Cu, Zn, Sn and S contents of the CZTS nanocrystals are reported in the formula given in table 2. Note that OH and C contents could be required to satisfy the electro-neutrality criteria. * EtOH: ethanol; i-PrOH: isopropanol; EG: ethylene glycol.

Solvent*	Reaction mixture composition (Cu:Zn:Sn)	OH:S	Nanocrystal composition
EtOH	(2.00:1.25:1.00)	1:5	$Cu_2Zn_{0.25}Sn_{1.02}S_{3.2}^{(1)}$
i-PrOH	(2.00:1.00:1.00)	2:7	$Cu_{2.00}Zn_{0.66}Sn_{1.16}S_{4.42}^{(2)}$
i-PrOH	(2.00:1.25:1.00)	2:7	$Cu_{2.00}Zn_{0.75}Sn_{1.19}S_{4.50}^{(2)}$
EG	(2.00:1.00:1.00)	1:5	$Cu_2Zn_{0.84}Sn_{0.97}S_{4.55}^{(1)}$
EG	(2.00:1.30:1.10)	0:5	$Cu_2Zn_{1.03}Sn_{1.09}S_{4.52}^{(1)}$
EG	(2.00:1.30:1.10)	1:5	$Cu_2Zn_{1.07}Sn_{1.05}S_{4.46}^{(1)}$
EG	(2.00:1.30:1.10)	2:5	$Cu_2Zn_{1.20}Sn_{0.94}S_{4.40}^{(1)}$
EG	(2.00:1.30:1.10)	5:5	$Cu_2Zn_{1.20}Sn_{0.94}S_{3.70}^{(1)}$
EG	(2.00:1.30:1.10)	2:7	$Cu_2Zn_{1.20}Sn_{1.14}S_{5.46}^{(1)}$
EG	(2.00:1.30:1.10)	3:7	$Cu_2Zn_{1.20}Sn_{0.98}S_{4.76}^{(1)}$

ratios, required for high-performance solar cells [29–31] were achieved from reaction mixtures possessing larger Zn and Cu compositions (Zn/Cu$_{molar}$ = 1.3 and Sn/Cu$_{molar}$ = 1.1).

Chemical analysis of CZTS samples prepared from reaction mixtures displaying increased thiourea content ([S]/[Cu] = 7) shows a large increase of sulfide content. This result is consistent with the larger content of amor-phous compounds determined in these samples by Raman spectroscopy. In contrast, an increase in OH concentration of the reaction mixtures results in a large decrease of the sulfide content of the synthesized CZTS samples. The much lower sulfide concentration than that required for electro-neutrality determined in these samples suggests the presence of OH content in the CZTS samples synthesized from reaction mixtures possessing [OH]/[Cu] > 2. For reaction mixtures with [OH]/[Cu] < 2, the sulfide content
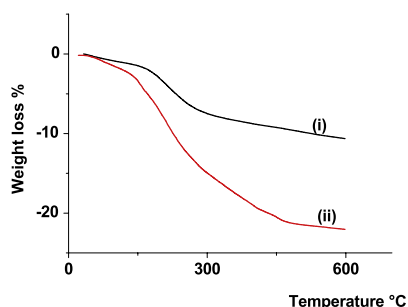
Figure 4. Thermogravimetric analysis (TGA) of CZTS crystals in N_2 atmosphere. $v = 1\,°C\,min^{-1}$ prepared by polycondensation in ethylene glycol at $T = 200\,°C$. (i) As-synthesized and after washing. (ii) After ball milling and size selection.


Figure 5. FTIR spectra of CZTS samples prepared in ethylene glycol at $200\,°C$ during 16 h. The spectra have been displaced vertically for clarity.

of these samples was slightly larger than that required for electro-neutrality, suggesting the presence of some sulfide-containing species probably arising from thiourea decomposition. Typical compositions exhibiting Cu deficiency ($Cu_2Zn_{1.07}Sn_{1.05}S_{4.5}$) required for high-performance solar cells were achieved for reaction mixtures possessing (Cu:Zn:Sn:S:OH) = (2.0:1.3:1.1:10:2.0) compositions. Preliminary investigations of these nonstoichiometric CZTS samples by coupled SEM–EDS characterization performed on polished samples composed of CZTS particles embedded in an organic resin suggest that the Cu deficiency and Zn over-stoichiometric ratio result from the formation of ZnS and SnS_2 secondary phases rather than Cu deficiency and Zn over-stoichiometric CZTS crystals. Thus, our results show that nonstoichiometry CZTS nanocrystals could not be synthesized at $200\,°C$ but rather include binary sulfide mixtures as reported in previous published works [11], Concerning the non-metallic elements, although a slight sulfur excess was determined in this latter sample ([S]/[Cu] = 4.5), carbon analysis indicates a molar carbon content C/Cu = 0.9 larger than the sulfur excess. This suggests the presence of derived thiourea compounds possessing a global C/S ratio, C/S > 1 or the presence of other species such as CNO^- in the CZTS samples.

Thermal gravimetric analysis (TGA) of CZTS samples performed under N_2 atmosphere up to $600\,°C$ reveals the presence of a significant proportion of volatiles (around 12 wt%) in the CZTS particles with a first significant weight loss occurring at a relatively low temperature, $T = 240\,°C$. This temperature, similar to the thiourea decomposition temperature [32] previously reported, indicates the presence of thiourea in the CZTS samples. Note that complete removal of the volatiles associated with a larger weight loss was achieved at $T = 600\,°C$ on similar samples but after fragmentation by ball milling (figure 4).

To better describe the identity of these volatile compounds, FTIR investigation was undertaken and has revealed the presence of various peaks with peak maxima at 3330, 1629, 1415, 1395 and 1110 cm^{-1} (figure 5). Similar peaks were also observed on CZTS samples synthesized in isopropanol, indicating that these peaks could not be assigned to the solvents. The spectra also exhibit a broad band around 3430 cm^{-1}. This band was previously reported
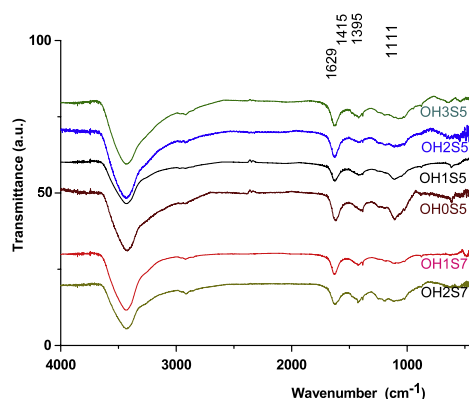
as an OH stretching vibrational band of H_2O or as the asymmetric and symmetric NH stretching vibrational bands of thiourea, with a slight shift observed to higher wavenumber assigned to the formation of the metal–thiourea complexes [33]. Peaks observed at 1629, 1415, 1395 and 1110 cm^{-1} were already reported and were attributed to metal–thiourea complexes [34]. A more complete assignment of these peaks was proposed from another investigation performed on metal–thiourea complexes [35] involving δ N–H bending deformation (1626 cm^{-1}), NH_2 rocking vibration, v C–S stretching vibration or N–C–N stretching vibration (1415, 1401 cm^{-1}), v C = S, v C–N or NH_2 rocking vibration (1105 cm^{-1}). In addition, after renormalization of the 3430 cm^{-1} peak intensity from the various FTIR curves, a broadening and a decrease of the intensity of the 1110 cm^{-1} peak are observed with increased OH and S additions ([OH]/[Cu] > 2 or [S]/[Cu] = 7) to the reaction mixture. These variations can be assigned to the formation of less well-defined metal–thiourea complexes, in association with the increased proportion of amorphous phase as previously shown by Raman spectroscopy.

While the overall composition of the partially crystallized nanoparticles exhibits the required chemical composition for high-performance CZTS absorbers, our experimental data indicate that the CZTS particles include thiourea or metal–thiourea complexes which could be removed at relatively low temperatures ($T < 300\,°C$).

3.4. Individualized CZTS nanoparticles: synthesis and characterization

As previously reported, the CZTS particles were formed either from ionic species, colloidal particles or slightly flocculated nanoparticles. Depending on the nature of the precursor, a large variation in the texture of the CZTS particles precipitated by temperature polycondensation was observed (figure 6). Compact aggregates were formed from ionic precursor solutions ([OH]/[Cu] = 0) whereas N_2 adsorption–desorption and TEM images (figure 7) demonstrated the formation of loosely packed aggregates for samples prepared from colloidal or slightly flocculated
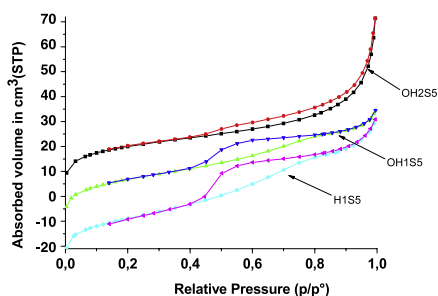
Figure 6. N$_2$ absorption–desorption curves recorded on CZTS samples prepared in ethylene glycol showing larger pore volume and larger pore size for samples synthesized from precursors prepared with increased OH addition. OH$_x$S$_y$ denotes [OH]/[Cu] = x and [S]/[Cu] = y. The curves have been displaced vertically for clarity.

precursors ([OH]/[Cu] = 1 or 2). An average pore diameter of 4 nm with corresponding surface area up to 72 m^2 g^{-1} was thus determined for samples synthesized at [OH]/[Cu] = 1 and [S]/[Cu] = 5 in ethylene glycol. By increasing the OH$^-$ content in the ((Cu^{2+})$_a$ (Zn^{2+})$_b$(Sn^{4+})$_c$ (Tu)$_d$ (OH$^-$)$_e$)$^{t+}$ precursor, an increase of both size and polydispersity of the CZTS pores was observed from N$_2$ adsorption–desorption isotherms.

The formation of a loosely packed CZTS aggregate from the ((Cu^{2+})$_a$ (Zn^{2+})$_b$(Sn^{4+})$_c$ (Tu)$_d$ (OH$^-$)$_e$)$^{t+}$ precursors probably involves SnO$_2$-rich colloidal seeds. Presence of these SnO$_2$-rich seeds into the precursors is suggested by the SnS$_2$ or SnS phases observed after calcination of the precursors as previously reported. The formation of loosely packed CZTS aggregates thus probably arises from the lesser mobility displayed by these SnO$_2$-rich seeds compared with non-hydroxylated metallic cations usually involved in classical solvothermal routes.

This systematic investigation has allowed us to better select the synthesis conditions to achieve formation of single-phase CZTS crystals displaying nearly stoichiometric composition and small primary crystallite sizes along with suitable short range order as characterized by Raman spectroscopy. Another crucial point to be considered, leading to the successful nanoparticle formation is the

achievement of loosely packed CZTS nanocrystals which can be easily fragmented further by ball milling. From all our results, optimal conditions for CZTS nanoparticle formation thus involve polycondensation of precursors synthesized at [OH]/[Cu] = 1 and [S]/[Cu] = 5 in ethylene glycol.

Our synthetic procedure involving polycondensation of ((Cu^{2+})$_a$ (Zn^{2+})$_b$(Sn^{4+})$_c$ (Tu)$_d$ (OH$^-$)$_e$)$^{t+}$ complexes ensures fast nucleation and an effective growth inhibition by adsorption of thiourea-derived species onto CZTS nanocrystal surfaces. The presence of these surface species results in electrostatic interactions between the CZTS surface-attached thiourea such that CZTS dispersions could be prepared. Dispersion of CZTS nanoparticles was investigated on ball-milled nanoparticles in various solvents within the framework of Hansen solubility parameter theory [36–38]. This investigation shows that the CZTS nanoparticles were successfully dispersed into various solvents displaying polar and H-bonding components within well-defined ranges. Dispersion and size selection of the CZTS nanoparticles were thus achieved in polar solvents such as ethanol, acetonitrile, ethylene glycol or dimethyl sulfoxide (DMSO), displaying hydrogen and polar Hansen solubility parameters, δH and δP, characterized by 22 < ($\delta H + \delta P$) < 30. In contrast to preliminary results [23], and from careful detailed investigations involving intense washing, a negative surface charge was determined by electrophoretic mobility measurements on CZTS nanocrystals. Because these CZTS nanocrystals displayed low surface charge as illustrated by the low value of the electrophoretic mobility (0.5 μm cm V^{-1} s^{-1}) determined in ethanol (figure S1 available at stacks.iop.org/Nano/23/185402/mmedia), stable CZTS dispersions were only achieved in low ionic strength suspensions. In a typical procedure, individualization of the loosely packed aggregates synthesized in ethylene glycol ([OH]/[Cu] = 1, [S]/[Cu] = 5) was achieved by ball milling into ethanol using 0.3 mm ZrO$_2$–Y$_2$O$_3$ balls. After intense washing decreasing the ionic strength of the suspensions, CZTS nanoparticles were size-selected in ethanol by centrifugation at 3000 rpm. The dispersed nanoparticles display an average particle size centered on 200 nm (figure S2 available at stacks.iop.org/Nano/23/185402/mmedia). This average size is
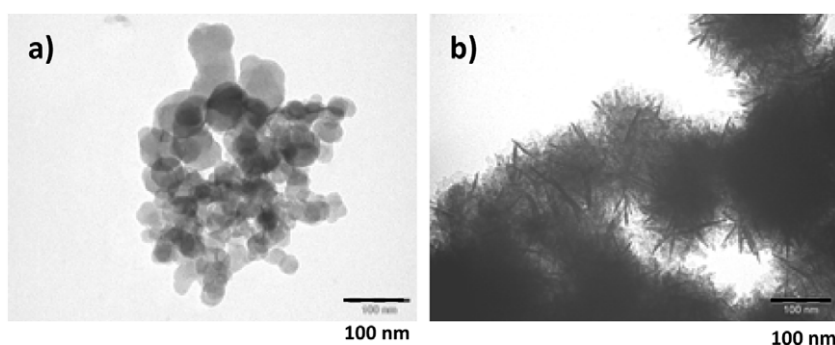
Figure 7. (a) TEM image of CZTS samples prepared in ethylene glycol showing loosely packed aggregates prepared by polycondensation of oxy-hydroxy-thiourea-M^{n+} precursors. (b) TEM image of reference sample prepared without any OH addition [OH]/[Cu] = 0 and [S]/[Cu] = 3 was reported for comparison. Scale bar: 100 nm.
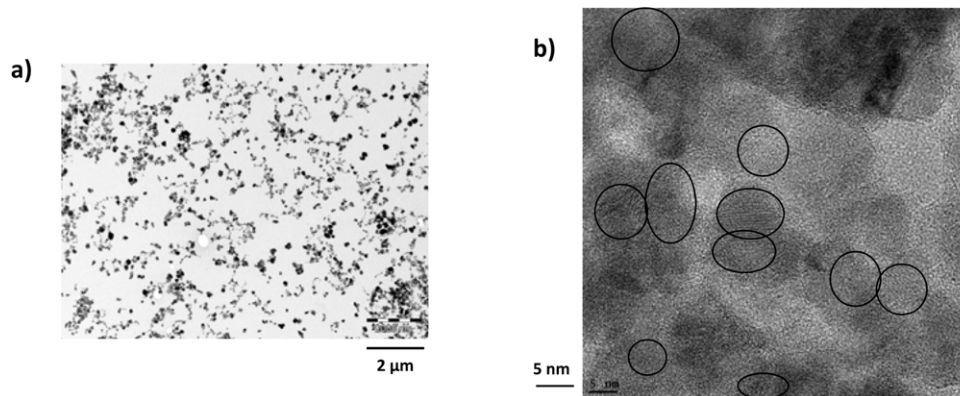
Figure 8. TEM images of CZTS nanoparticles synthesized in ethylene glycol, $T = 200\,°C$. (a) Low magnification image showing a large number of individualized CZTS nanoparticles dispersed in ethanol. Scale bar 2000 nm. (b) High resolution TEM image showing primary crystallites embedded in amorphous domains. Scale bar is 5 nm.

consistent with the low magnification TEM images showing that these nanoparticles indeed consist of individualized aggregates of 150–300 nm size. High resolution TEM images (figure 8) clearly reveal that these aggregates are composed of both 5–10 nm size primary crystallites and amorphous domains localized on the outer surface or mixed with crystallized nanodomains. Moreover, as shown by Raman and TEM images, the presence of a larger proportion of these amorphous domains on samples synthesized in similar conditions but at a lower temperature (150 °C) suggests that these amorphous domains probably consist of $((Cu^{2+})_a (Zn^{2+})_b (Sn^{4+})_c (Tu)_d (OH^-)_e)^{t+}$ complexes which further transform into CZTS crystallites.

Design and polycondensation of tailored complex precursors $((Cu^{2+})_a (Zn^{2+})_b (Sn^{4+})_c (Tu)_d (OH^-)_e)^{t+}$ formed from metallic cations and controlled additions in a very narrow range of OH^- anions and thiourea yield loosely packed aggregates resulting in the synthesis of surfactant-free CZTS nanoparticles. Thus, our process route was designed by employing a sulfide source which acts both as a complexing agent inhibiting crystallite growth and as a surface additive for redispersion in low ionic strength polar solvents. Another advantage is the easy removal of thiourea by heat treatment at relatively low temperatures ($T < 300\,°C$) as demonstrated from TGA curves, indicating that thiourea behaves as a transient additive.

From the UV–vis curve recorded on the calcined CZTS nanoparticles, we have determined a bandgap of 1.5 eV, in agreement with the values already reported [4, 5] (figure S3 available at stacks.iop.org/Nano/23/185402/mmedia).

3.5. Formation of crack-free CZTSe films from partially crystallized CZTS nanoparticles

Fabrication of the crack-free sintered CZTSe absorber layer is required since the cracks induce solar cell short-circuits. Crack formation can arise during the film forming stage as well as during the sintering stage. Crucial parameters leading to the formation of crack-free green films using nanoparticle building blocks have largely been investigated [39, 40]

highlighting the dramatic effect of capillary stresses when employing nanosized particles. Corresponding crack-free sintered films have also been reported involving a Se vapor phase sintering mechanism [12]. Because our building blocks yield a low green density film and thus undergo a significant shrinkage during sintering, fabrication of crack-free films using our partially crystallized CZTS nanoparticles remains a challenging task.

Our approach to fabricate films involves, in a first stage, the preparation of a highly concentrated CZTS dispersion. Colloidal stabilization of the CZTS nanoparticles was first improved by replacing organic surface species previously described with an organic-free ligand such as a S^{2-} anion [41]. This ligand substitution was carried out by solution exchange using aqueous $(NH_4)_2S$ solution at room temperature yielding a significant increase of the ζ potential for S^{2-}-capped CZTS nanocrystals in H_2O and in EtOH (-50 mV). While decreasing significantly the thiourea content of the building blocks, this increase in nanocrystal electrostatic stabilization enables the formation of stable concentrated CZTS (up to 100 g l^{-1}) dispersions. We have thus explored the formation of CZTS crack-free films on Mo-coated glass substrates by dip coating into CZTS dispersions. In a second stage, since our partially crystallized building blocks yield low green density films, we have explored intermediate heat treatments at $T > 250\,°C$ under Ar atmosphere to decrease shrinkage during sintering. The significant decrease of the intensity of the various peaks assigned to C = S, C–N and N–H vibrations with increased heat treatment temperatures (figure S4 available at stacks.iop.org/Nano/23/185402/mmedia) as observed in FTIR spectra recorded on the heat-treated films confirms the organic volatile compounds removal as shown from TGA curves. X-ray diffraction patterns recorded on various films calcined under Ar atmosphere at various temperatures during 6 h (figure S5 available at stacks.iop.org/Nano/23/185402/mmedia) reveals a crystallite growth onset temperature around 350 °C. The slight increase of the x-ray-ordered domain size from 7 nm (as-synthesized) to 8.5 nm ($T = 350\,°C$) indicates that these intermediate heat treatments do not significantly
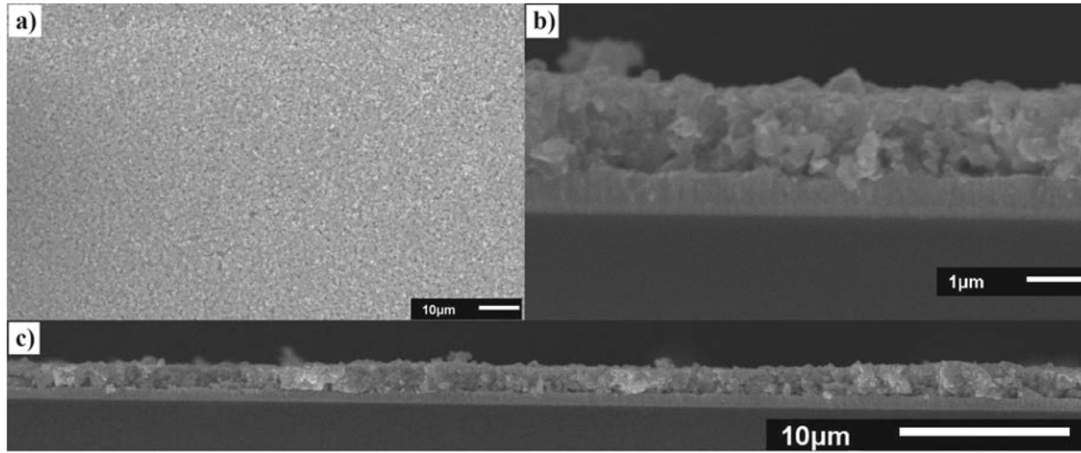
Figure 9. SEM images of CZTSe films sintered at $T = 550\,°C$. (a) Low magnification image showing a crack-free film. (b) Cross-section high magnification image showing 1.5 μm thickness and CZTS layer microstructure. (c) Typical cross-section low magnification image showing uniform thickness of sintered CZTSe films.

alter the driving force for sintering enabling large grain microstructure. Finally, successful preparation of crack-free films was achieved using concentrated, ethanolic, stable dispersions when the films are fabricated with a thickness lower than the critical film thickness [39]. Since this critical thickness, e_{crit}, was determined for our dispersions in the range 600–800 nm, several successive layers were required to achieve 1.5 μm thickness sintered films. Figure 9 shows images of a typical CZTSe sintered crack-free film fabricated with nine deposited layers. As a proof of concept, intermediate heat treatments were performed after three successive layers at a relatively high temperature, $T = 400\,°C$, to facilitate film pre-densification and removal of volatiles. A low magnification image of the film sintered at $T = 550\,°C$ reveals a uniform crack-free film while a high magnification image shows the presence of grains of approximately 300 nm size. Optimizations of intermediate heat treatment temperature and of recrystallization processing of the film are under progress with the objective to achieve larger grain microstructure.

Despite the large shrinkage inherent in the densification of a low density green film, we thus demonstrate the ability to achieve a crack-free CZTSe film when using partially crystallized CZTS building blocks.

3.6. Low-defect concentration CZTSe sintered films

High-performance solar cells rely on the fabrication of low-defect concentration absorbers. A significant decrease of the organic impurity content of the nanoparticle building blocks has first been achieved by S^{2-} solution exchange. Additional decrease of the carbon content of the CZTSe film was also observed during the sintering performed at $T = 550\,°C$ under Se atmosphere. Typically, sintered films fabricated using (Cu:Zn:Sn:S) = (2:1.3:1.1:1) composition possess $Cu_2ZnSnSe_4$ as a main phase along with minor content of non-converted Cu_2ZnSnS_4 as shown by Raman spectroscopy (figure S6 available at stacks.iop.org/Nano/23/185402/mmedia). Note that any secondary phase such as ZnSe was observed by Raman spectroscopy. The proportion of the main $Cu_2ZnSnSe_4$ phase was determined by EDS showing an atomic ratio $[Se]/([S] + [Se]) = 0.80$. Although in these preliminary experiments, our sintered films did not exhibit the optimum microstructure with large grains (figure 9), optoelectronic characteristics of CZTSe films sintered under Se atmosphere at $550\,°C$ for 1 h were explored by photoluminescence spectroscopy from 10 to 300 K. Using 1.652 eV laser irradiation, a clear photoluminescence signal was recorded with a peak maximum centered at 0.98 eV at $T = 10$ K, close to the bandgap value of CZTSe (1.02 eV) [6] (figure 10). Indeed, previous work has shown that the presence of defects decrease this peak energy. For instance, a photoluminescence band at 0.946 eV at 10 K was determined in $Cu_2ZnSnSe_4$ monograins [42] and attributed to a band to impurity recombination in CZTSe. Therefore the PL peak energy determined here, close to the bandgap value, indicates that our sintered films prepared from partially crystallized building blocks possess a rather low defect content. These results are encouraging since it was recently demonstrated that a significant photovoltaic effect in CZTS can only be observed in solar cells exhibiting a PL peak close to the bandgap energy. Lower quality CZTS solar cells with very low efficiency exhibit a weak and broad PL with a peak located a few hundred meV below the gap [43]. The carrier lifetimes have been measured by TRPL spectroscopy, as it has been demonstrated to be a suitable characterization tool for the identification of promising absorbing materials [44]. Figure 10(b) shows the representative PL decay curves of the CZTSe film which was measured at the emission peak energy at 10 K and room temperature. The carrier lifetimes extracted from these curves are $\tau_1 = 500$ ps and $\tau_2 = 120$ ps, respectively, at 10 K and 300 K. The PL decay time is still limited by the recombination of the photogenerated carriers on non-radiative defects, as confirmed by the loss of the PL time-integrated intensity by one order of magnitude between 10 K and 300 K (figure 10(a)). Nevertheless, values larger than 100 ps clearly demonstrate the reasonable electronic properties of the synthesized material. These lifetimes could be greatly improved through an optimization
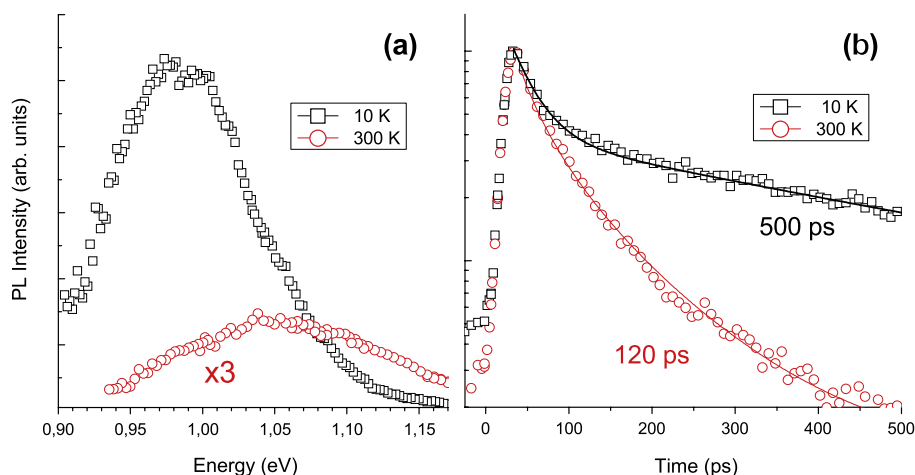
Figure 10. (a) PL and (b) TRPL characteristics of CZTSe films sintered at 550 °C 1 h under Se atmosphere.

of the sintering stage yielding larger grain microstructure. Although high-performance CZTSe absorbers show a longer carrier lifetime of 1.2 ns [45], our decay time recorded on a non-optimized microstructure suggests that our partially crystallized building blocks can be useful for the fabrication of solar cells.

4. Conclusions

Solvothermal syntheses of complex metallic sulfides generally yield micron-sized compact aggregates. Design of tailored complex precursors $((Cu^{2+})_a\ (Zn^{2+})_b(Sn^{4+})_c\ (Tu)_d\ (OH^-)_e)^{t+}$ formed from metallic cations and controlled addition in a very narrow range of OH^- anions and thiourea as sulfide source followed by their polycondensation has allowed the fabrication of partially crystallized CZTS nanoparticles. Using this simple sulfide source, we developed an attractive process route taking advantage of thiourea both as a complexing agent inhibiting crystallite growth, and as a surface additive providing redispersion in low ionic strength polar solvents. In the context of the potential large scale deployment of photovoltaic cells, this work addresses the issue of costs involving both low-cost raw materials and the use of thiourea as a multifunctional additive. In addition, the easy removal of thiourea by S^{2-} post-exchange has allowed us to achieve more stable CZTS dispersions in a usual polar solvent such as ethanol. Coupled to this carbon purification of the nanoparticle building blocks using the S^{2-} exchange, a specific film-forming procedure was proposed involving highly concentrated, surfactant-free, binder-free CZTS dispersions resulting in crack-free green films. The ability to fabricate low-defect-concentration, crack-free, sintered films from these surfactant-free CZTS nanoparticles represents a promising strategy for the manufacture of low-cost and high-performance CZTSe absorbers.

Acknowledgments

References

[1] Ito K and Nakazawa T 1988 *Japan. J. Appl. Phys.* **27** 2094
[2] Katagiri H, Sasaguchi N, Hando S, Hoshino S, Ohashi J and Yokota T 1997 *Sol. Energy Mater. Sol. Cells* **49** 407
[3] Scragg J J, Dale P J, Peter L M, Zoppi G and Forbes I 2008 *Phys. Status Solidi* b **245** 91772
[4] Jimbo K, Kimura R, Kamimura T, Yamada S, Maw W S, Araki H, Oishi K and Katagari H 2007 *Thin Solid Films* **515** 5997
[5] Zhang J, Shao L, Fu Y and Xie E 2006 *Rare Met.* **25** 315
[6] Katagiri H, Jimbo K, Yamada S, Kamimura T, Maw W S, Fukano T, Ito T and Motohiro T 2008 *Appl. Phys. Expr.* **1** 041201
[7] Araki H, Kubo Y, Mikaduki A, Jimbo K, Maw W S, Katagiri H, Yamazaki M, Oishi K and Takeuchi A 2009 *Sol. Energy Mater. Sol. Cells* **93** 996
[8] Scragg J J, Dale P J and Peter I M 2009 *Thin Solid Films* **517** 1241
[9] Guo Q, Hillhouse H W and Agrawal R 2009 *J. Am. Chem. Soc.* **131** 11672
[10] Steinhagen C, Panthani M G, Akhavan V, Goodfellow B, Koo B and Korgel B A 2009 *J. Am. Chem. Soc.* **131** 12554
[11] Todorov T K, Reuter K B and Mitzi D B 2010 *Adv. Mater.* **22** 1
[12] Guo Q J, Ford G M, Yang W C, Walker B C, Stach E A, Hillhouse H W and Agrawal R 2010 *J. Am. Chem. Soc.* **132** 17384
[13] Riha S C, Parkinson B A and Prieto A L 2009 *J. Am. Chem. Soc.* **131** 12054
[14] Shavel A, Arbiol J and Cabot A 2010 *J. Am. Chem. Soc.* **132** 4514
[15] Nanosolar Inc. 2007 PVSEC 17 Tokyo, Japan
[16] Yu S H, Coelfen H and Fisher A 2004 *Coll. Surf.* A **243** 49
[17] Chatry M, Henry M, In M, Sanchez C and Livage J 1994 *J. Sol–Gel Sci. Technol.* **1** 233
[18] Buissette V, Moreau M, Gacoin T, Boilot J P, Chane-Ching J Y and Lemercier T 2004 *Chem. Mater.* **16** 3767
[19] Gonzalez-McQuire R, Chane-Ching J Y, Vignaud E, Lebugle A and Mann S 2004 *J. Mater. Chem.* **14** 2277
[20] Guha P, Gorai S, Ganguli D and Chaudhuri S 2003 *Mater. Lett.* **57** 1786
[21] Hu H, Yang B, Liu X, Zhang R and Qian Y 2004 *Inorg. Chem. Commun.* **7** 563

[22] Gou X, Peng S, Zhang L, Shi Y, Chen J and Shen P 2006 *Chem. Lett.* **35** 91050

[23] Zaberca O, Gillorin A, Durand B and Chane-Ching J Y 2011 *J. Mater. Chem.* **21** 6483

[24] Fernandes P A, Salome P M and Da Cunha A F 2009 *Thin Solid Films* **517** 2519

[25] Fontane X, Calvo-Barrio L, Izquierdo-Roca V, Saucedo E, Perez-Rodriguez A, Morante J R, Berg D M, Dale P J and Siebentritt S 2011 *Appl. Phys. Lett.* **98** 181905

[26] Zwick A and Carles R 1993 *Phys. Rev.* B **48** 6024

[27] Shuker R and Gammon R W 1970 *Phys. Rev. Lett.* **25** 222

[28] Himmrich M and Haeuseler H 1991 *Spectrosc. Acta* A **47** 7933

[29] Katagiri H, Jimbo K, Tahara M, Araki H and Oishi K 2009 *Mater. Res. Soc. Symp. Proc.* **1165** 04

[30] Nagoya A and Asahi R 2010 *Phys. Rev.* B **81** 113202

[31] Chen S, Gong X G, Walsh A and Wei S H 2010 *Appl. Phys. Lett.* **96** 021902

[32] Madarasz J and Pokol G 2007 *J. Thermal Anal. Calor.* **88** 2329

[33] Gorai S, Ganguli D and Chaudhuri S 2005 *Cryst. Growth Des.* **5** 3875

[34] Das K, Panda S K, Gorai S, Mishra P and Chaudhuri S 2008 *Mater. Res. Bull.* **43** 2742

[35] El-Bahy G M S, El-Sayed B A and Shabana A A 2003 *Vib. Spectrosc.* **31** 101

[36] Bergin S D, Sun Z Y, Streich P, Hamilton J and Coleman J N 2009 *ACS Nano* **3** 2340

[37] Hansen C M 2007 *Hansen Solubility Parameters—A User's Handbook* (Boca Raton, FL: CRC Press)

[38] Hildebrand J H, Prausnitz J M and Scott R L 1970 *Regular and Related Solutions* (New York: Van Nostrand Reinhold Company) p 228

[39] Man W and Russel W B 2008 *Phys. Rev Lett.* **100** 198302

[40] Singh K B, Bhosale L R and Tirumkudulu M S 2009 *Langmuir* **25** 4284

[41] Nag A, Kovalenko M V, Lee J S, Liu W, Spokoyny B and Talapin D V 2011 *J. Am. Chem. Soc.* **133** 10612

[42] Grossberg M, Krustok J, Timmo K and Altosaar M 2009 *Thin Solids Films* **517** 2489

[43] Romero M J, Du H, Teeter G, Yan Y and Al-Jassim M M 2011 *Phys. Rev.* B **84** 165324

[44] Ohnesorge B, Weigand R, Bacher G, Forchel A, Riedl W and Karg F H 1998 *Appl. Phys. Lett.* **73** 1224

[45] Gunawan O, Todorov T K and Mitzi D B 2010 *Appl. Phys. Lett.* **97** 233506